HiSST: 2nd International Conference on
High-Speed Vehicle Science Technology
11–15 September 2022, Bruges, Belgium

HEXAFLY-INT: Design of the Experimental Flight Test Vehicle

Sara Di Benedetto [1], Salvatore Cardone[2], Gianfranco Morani[1], Antonio Schettino[1], Marco Marini[1], Roberto Scigliano[1], Domenico Cristillo[1], Paolo Vernillo[1], Roberto Fauci[1], Breno de Oliveira e Silva [3], Lucas Galembeck[3], Victor F. Villace[4], Johan Steelant[4]

Abstract

This paper will provide a comprehensive description of the multidisciplinary activities performed in the frame of the HEXAFLY-INT project in order to design both the mission and the vehicle (Experimental Flight Test Vehicle, EFTV) with the aim at designing an unpowered controlled flight test at hypersonic speed, demonstrating the capability of performing manoeuvres and carrying on-board breakthrough technologies.
The payload will be launched by the Brazilian VS-50 launcher, performing a suborbital trajectory, and being released at 90 km. During the early phase of its descent flight segment, the EFTV will be docked to the Experimental Support Module (ESM) which has the aim of controlling the vehicle attitude by means of Cold Gas reaction control System thrusters (CGS). After the separation from the ESM, a pull-out manoeuvre will bring the EFTV to level flight condition at a target altitude of 32km at approximately Mach 7 (experimental phase).
A synthesis of the relevant aspects, means and methodologies used for assessing EFTV's aerodynamic behaviour and aerothermodynamic features, materials and thermal protection system, structural loads and stress analysis, and trajectory is reported. All these aspects depend on each other and together they lead to the definition of the vehicle and the mission matching the initial requirements.
The final aim of the activity is to define methods and standards for different critical aspects of high-speed flying systems, and then to collect valuable flight data to validate methods and technologies in a dedicated experimental flight campaign.

Keywords: *Hypersonics, Flight test, Vehicle design, High Speed Transportation*

Nomenclature

Latin
a - Accelerations
AoA – Angle of Attack
AEDB – Aerodynamic Database
CAD – Computer Aided Design
CAE - Computer Aided Engineering
CDR – Critical Design Review
IMU – Inertial Measurement Unit
LRF – Layout Reference Frame
M – Mach number
MCI – Mass, Centre of Gravity, Inertia
MoS – Margin of Safety
Nz, Ny – Inertial loads
p - Pressure

[1] *Centro Italiano Ricerche Aerospaziali (CIRA), Via Maiorise 81043, Capua (CE), Italy, s.dibenedetto@cira.it, a.schettino@cira.it, m.marini@cira.it, r.scigliano@cira.it, f.nebula@cira.it, g.morani@cira.it, d.cristillo@cira.it, p.vernillo@cira.it, r.fauci@cira.it*
[2] *Tecnosistem Engineering and Technology (TET), vico II S. Nicola alla Dogana, 80133 Napoli, scardone@tecnosistemspa.it*
[3] *Instituto de Estudos Avançados (IEAv), Institute for Advanced Studies, São José dos Campos, SP, Brazil, brenobos@ieav.cta.br, galembecklg@fab.mil.br*
[4] *European Space Agency (ESA-ESTEC), Keplerlaan 1, 2200 AG Noordwijk, The Netherlands, Victor.Fernandez.Villace@esa.int, Johan.Steelant@esa.int*

CFD – Computational Fluid Dynamics
CGS – Cold Gas System
CLA – Centro de Lançamento de Alcântara
CMC – Ceramic Matrix Composite
CoG – Centre of Gravity
CTR - Central
Dof – Degree of freedom
DPL – Descent Phase Loads
EC – European Commission
EFTV - Experimental Flight Test Vehicle
ESM – Experimental Support Module
FCC – Flight Control Computer
FEM – Finite Element Model
FPA – Flight Path Angle
FWD - Forward
GNC – Guidance Navigation and Control
HEXAFLY – High-Speed Experimental Fly Vehicle
P – Position
PDR – Preliminary Design Review
PVA – Position, Velocity, Attitude
Q – Heat flux
QR – Qualification Review
RANS – Reynolds Averaged Navier-Stokes
RWD – Rear
SF – Skin Friction
SM – Static Margin
T - Temperature
TPS - Thermal Protection System
V - Velocity

Greek

δ – Trim deflection
Δ – Error
ε – Emissivity coefficient
χ – Track angle
σ - Stresses

1. Introduction

Civil High-speed transportation has always been hampered by the lack of range potential or a too high fuel consumption stemming from a too low cruise efficiency. Indeed, looking into the performance of classically designed high-speed vehicles, their performances drop nearly linearly with flight Mach number as indicated by the red line on Fig 1 [1]. Over the last years, however, radical new vehicle concepts were proposed and conceived having a strong potential to alter this trend. This innovative approach is based upon a well elaborated integration of a highly efficient propulsion unit with a high-lifting vehicle concept. The realization of both a high propulsive and aerodynamic efficiency is based upon the minimization of kinetic jet losses while striving to the best uniformity but minimal induced velocity for lift creation. The dashed green line in Fig 1 illustrates the potential of this innovative design methodology whereas the green line indicates what has been achieved as a revolutionary, high speed civil air transportation concepts worked-out along this new approach.
Performing a flight test will be the only and ultimate proof to demonstrate the technical feasibility of these new promising high-speed concepts versus their potential in range and cruise. This would result into a major breakthrough in high-speed flight and create a new era of conceptual vehicle designs.
At present, the promised performances can only be demonstrated by numerical simulations or partly experimentally. As high-speed tunnels are intrinsically limited in size or test duration, it is nearly impossible to fit even modest vehicle planform completely into a tunnel. Though numerical simulations are less restrictive in geometrical size, they struggle however with accumulated uncertainties in their modelling of turbulence, chemistry etc., thus making complete Nose-to-Tail predictions doubtful without in-flight validation. As a consequence, the obtained technology developments are now limited to a technology readiness level of TRL=4 (components validated in laboratory).
The HEXAFLY-INT project [2] aims to test one of these radically new conceptual designs accompanied with several breakthrough technologies on board of the high-speed vehicle in free flight. This approach will drastically increase the Technology Readiness Level (TRL) up to 6 (System demonstrated in relevant environment).
The design of a high-speed vehicle is characterized by continuous interactions between engineering disciplines, and therefore a multidisciplinary approach is needed.
The work described in this paper is focused on:

- the definition of system engineering procedures for designing a hypersonic unpowered glider and its experimental mission;
- the definition of a proper in-flight measurement system for the validation of numerical codes and tools, and more in general of hypersonic technologies, with experimental flight data, thus enabling future trans-atmospheric flights.

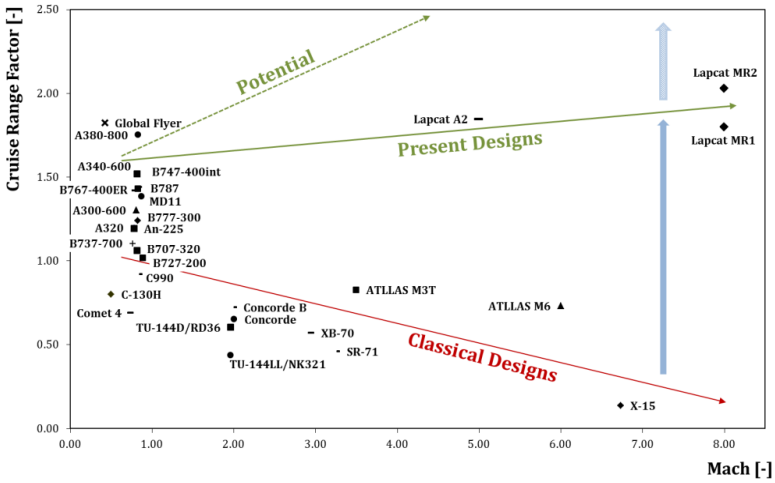

Fig 1. Long-range potential of high-speed vehicles in function of flight Mach number: Red: achievable with classical designs with minimal integration; Green: present designs based upon strongly integrated propulsion-vehicle designs with a potential limit (dashed line) [1].

The work stems from the interest of Europe in hypersonic civil transportation vehicles. In the past ten years projects like LAPCAT I and LAPCAT II [3, 4], as well as ATLLAS I & II [5, 6], helped to identify the major challenges in the development of hypersonic vehicles for long distance civil transport. Among the major technology challenges, the application of high-temperature materials originally developed for single use applications (e.g. re-entry vehicles) is currently under investigation for the long-life benefit and multiple mechanical-thermal cycles withstanding capability [7].

The current HEXAFLY-INT project [2], whose main results are described in this work, aims to demonstrate the feasibility of different critical aspects in a dedicated experimental flight campaign and collect valuable flight data to validate methods and technologies suitable for high-speed flying systems. The project, co-funded by the European Commission (EC) and the European Space Agency (ESA), is currently involving partners from Europe, Russian Federation, Australia and Brazil, operating under ESA/ESTEC coordination. The activity described in the paper has been carried out during the Phase C of the project, successfully concluded with the closure of the project's Critical Design Review.

The HEXAFLY Experimental Flight Test Vehicle (EFTV) is planned to be launched by the Brazilian VS50 launcher, equipped with a S50 rocket engine, which will perform a suborbital trajectory having an apogee at 90 km. During the early phase of its descent flight segment, the EFTV will be docked to the Experimental Service Module (ESM), which has the aim of controlling the vehicle attitude by means of cold gas Reaction Control System thrusters (RCS). After the separation from the ESM, a pull-out manoeuvre will bring the EFTV to level flight condition at a target altitude of 32km where the experimental phase will start in controlled hypersonic cruise at approximately Mach 7.
The main technical challenges of the project are specifically related to the design of the vehicle gliding configuration and the complexity of integrating breakthrough technologies with standard aeronautical technologies, e.g. high temperature protection system and airframe cold structures.

2. Flight Scenario and Experimental Flight test Vehicle

The HEXAFLY-INT payload will be launched by a sounding rocket, the Brazilian VS50 launcher equipped with a solid rocket motor, in a suborbital trajectory having an apogee at around 90 km and Mach 8.
A qualitative mission scenario is described in Fig 2. The vertical launch is planned from the Centro de Lançamento de Alcântara (CLA) in Brazil.
After the release from the launch vehicle, the Experimental Flight Test Vehicle (EFTV) will perform the early descent flight docked to a service module, namely the Experimental Support Module (ESM), which will control vehicle's attitude by means of a cold gas system (CGS) when the too low dynamic pressure does not allow controlling the vehicle by aerodynamic surfaces. As soon as the EFTV features complete aerodynamic control authority, it will undock from the ESM (at about 55km altitude) and it will pull up from its descent to perform a hypersonic cruise at approximately Mach 7 and at an altitude of about 32km. In this experimental window, the EFTV is expected to demonstrate a high aerodynamic efficiency

(L/D ≥ 4), a positive aerodynamic balance at controlled cruise Mach numbers (7÷8) and an optimal use of advanced high-temperature materials and structures.
Furthermore, the EFTV will perform a controlled hypersonic banking manoeuvre just after the pull-out manoeuvre, also to fly within the telemetry covered area (a 600 km radius circle with the town of Fortaleza as centre), and to end the mission at about Mach=2 and 20 km altitude.

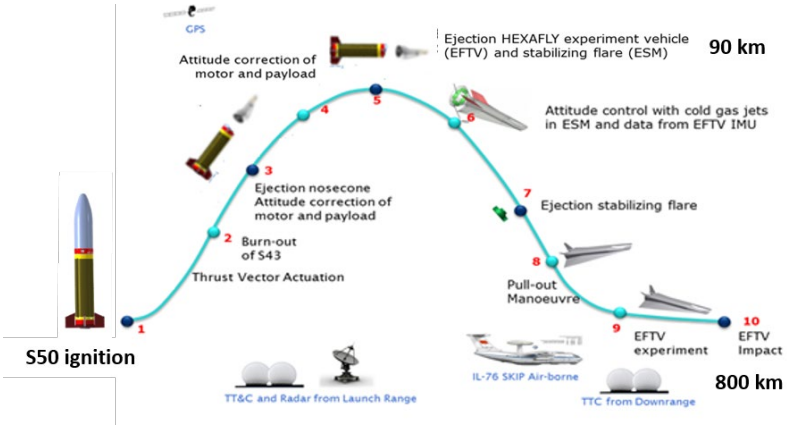

Fig 2. HEXAFLY-INT VS50 launch vehicle sketch (left) and qualitative mission scenario (right)

All the mission objectives and constraints, which have driven the vehicle design and the selection of the design methods detailed in section 3, are summarized in Table 1 for the different phases of the EFTV flight, where flight phases are defined as:

Phase 0: starting from the release from the ESM at 55km, and ending at 33km.
Phase I: level flight; starting from end of Phase 0 and ending when either Mach is under 6.5 or altitude is below 27km.
Phase II: gliding flight; starting from end of Phase I till splash-down.

The full payload composed by EFTV and ESM is shown in Fig 3. The EFTV is a hypersonic glider 3.29m long and with a wing span of about 1.23m [2]. It has a two-dimensional nosetip with 2mm rounding and 2mm lateral fillet, while the wing is characterized by an 80-deg sweep angle and 14-deg negative dihedral angle, and 1mm rounded leading edge. As control surfaces, the vehicle is equipped by a couple of active ailerons (0.4m long and 0.32m wide), which can be deflected in symmetric and asymmetric way, and a couple of fixed vertical fins characterized by a 68.5-deg sweep angle and a 54-deg angle formed between the two fins in the transversal plane.
As general material layout, the cold structure of the EFTV is in titanium alloy, as well as the entire fuselage, the wing panels and the fins, with the exception of the copper nose. C/C-SiC is the material for the hot wing leading edges and ailerons. The metallic exposed surface parts will be covered, in the most critical regions, by ZrO_2 coating with a proper optimized thickness. Moreover, high emissivity paint will be used to globally reduce surface temperatures and optimize the structure.

The EFTV will be equipped with an avionic system composed by an inertial measurement unit (IMU), a GPS, two servo-actuators for the ailerons, and a flight control computer (FCC) which will ensure the on-board mission management. The vehicle will also be equipped with an in–flight measurement system which will acquire pressure, temperature and acceleration data sensors for the sake of post flight analysis and simulation tools validation. The on-board avionics will also include a downlink telemetry system (i.e. with some antennas) which will transmit all mission data to the Ground Control Station located at the launch site.

Table 1: Mission requirements

Phase 0

	Constraint Value
Convective heat flux parameter ρ*v [kg/m^2/s]	< 75
Hinge Moment [Nm]	< 332 along the whole trajectory
Distance from Alcantara, Fortaleza or Natal [km]	< 600
Distance from the coast [km]	> 100 along the whole trajectory
Trim deflection range [deg]	> -20 and <10 along the whole trajectory

Phase I

	Constraint Value
Convective heat flux parameter ρ*v [kg/m^2/s]	< 75
Hinge Moment [Nm]	< 332 along the whole trajectory
Aerodynamic efficiency	> 4 for at least 3s
Flight Mach number [-]	6.5 < M <8
Flight path angle [deg]	< 5
Altitude [km]	> 27 and <33
Distance from Alcantara, Fortaleza or Natal [km]	< 600
Distance from the coast [km]	> 100 along the whole trajectory
Trim deflection range [deg]	> -20 and <10 along the whole trajectory

Phase II

	Constraint Value
Hinge Moment [Nm]	< 332 along the whole trajectory
Flight Mach number [-]	2 < Ma <6.5
Downrange [km][5]	> 500km
Cross range [km][6]	> 50km
Distance from Alcantara, Fortaleza or Natal [km]	< 600 along whole trajectory
Distance from the coast [km]	> 100 along the whole trajectory
Final Heading[7] [deg]	-40
Final Heading error [deg][8]	< 2
Trim deflection range [deg]	> -20 and < 10 along the whole trajectory

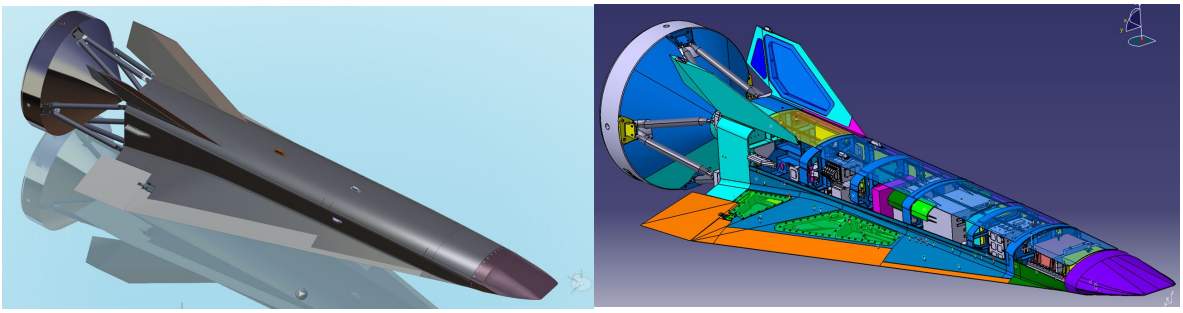

Fig 3. HEXAFLY-INT payload (EFTV+ESM). Right: internal view

3. Description of Methods

Methods and means for designing hypersonic vehicle and mission are described in the next sections. The approach defined is based on the tight interaction between subsystems up to completion of system and mission design, as described in the flow chart below (see Fig 4).
The process is coordinated by the system, which represents also the design authority, to fulfill the mission and system requirements reported in Table 1.

[5] Distance between two planes, both of them perpendicular to the initial orbital plane: the first plane goes through the Phase II start point and the local vertical and the second one passes through the Phase II end-point and is parallel to the first one.
[6] Minimum distance between Phase II end point and the initial orbital plane.
[7] From East, positive counter clockwise. The vehicle should end the flight parallel to the coast.
[8] The requirement of flying parallel to the coast was stated without accuracy requirements. CIRA assumed a maximum error w.r.t. a desired final heading angle.

The flow chart clarifies how, in the multidisciplinary approach, each discipline interacts with the other ones and with the system, and which parameters are being exchanged.

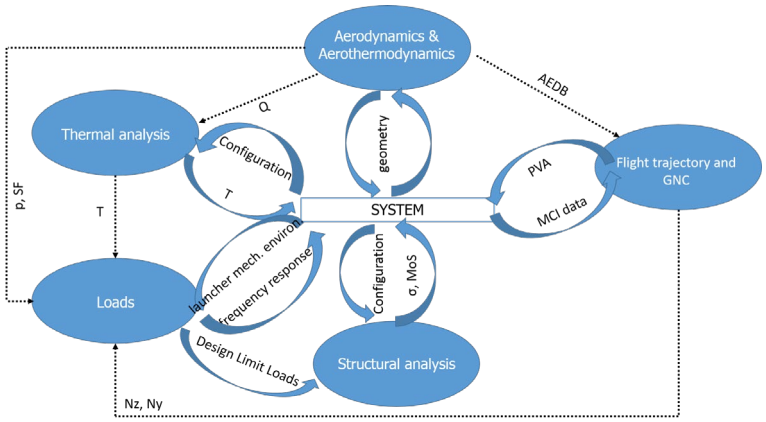

Fig 4. Multidisciplinary interactions and interdependencies within the different disciplines

3.1. Aerodynamic and aerothermodynamic design

A synthesis of the relevant aspects concerning the EFTV's aerodynamic and aerothermodynamic design is provided hereinafter, whereas more details can be found in Refs. [8, 9, 10, 11, 12, 13]. The EFTV aerodynamic database relies on a massive number of full three-dimensional Navier-Stokes CFD computations (more than 200) in order to build the Aerodynamic Model (AM) and the related Uncertainty Model (UM).

The aerodynamic behavior of EFTV was investigated in the light of a space-based design approach, while the vehicle's aerothermal loading environment was addressed with the trajectory-based approach. These results were used for the thermal analyses described in section 3.2.

An extensive comparison between numerical and experimental aerodynamic results was performed, these latter from the supersonic/hypersonic wind tunnel T-116 glider test campaign performed at TsAGI. This allowed to validate CFD results in representative conditions, and to define a suitable uncertainty model provided to Flight Mechanics along with the nominal aerodynamic coefficients [12].

Aerodynamic force and moment coefficients output of the numerical and experimental investigations were collected, and properly elaborated, to provide the EFTV aerodynamic model and, finally, the glider aerodynamic database (AEDB). The estimation of the boundary layer transition onset and extent as well as its receptivity due to imperfections are detailed in [13]. Further details about the methodology are provided in Ref. [12].

An example of the EFTV longitudinal aerodynamic characteristics in clean configuration for hypersonic aerodynamics (M_∞=7.0) is reported in Fig 5.

As far as CFD aero-heating results are concerned, computed surface distribution of radiative equilibrium temperature for one of the B-viscous (early reference) trajectory flight points is provided in Fig 6.

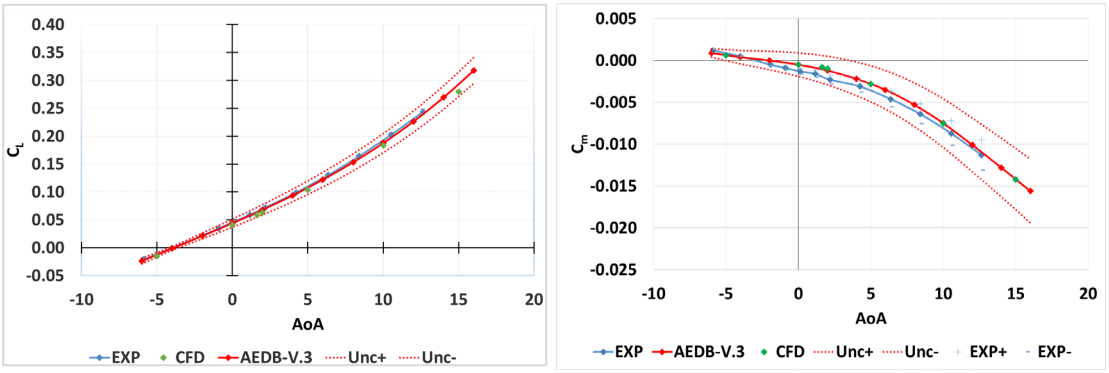

Fig 5. Lift and pitching moment coefficients at M_∞=7, β=0°, clean configuration.

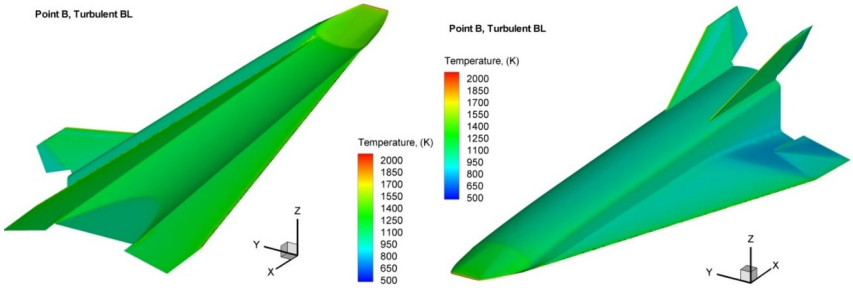

Fig 6. Temperature contours for the EFTV-071 flight point for fully turbulent flow

As shown in Fig 6, typically the glider features local overheating at nosetip, wing and fin leading edges as result of nearly attached shock waves. Results comparison between laminar and turbulent boundary layers indicates that heat flux at fuselage leading edge reaches values close to about 500 kW/m^2 at peak heating conditions, while a 300 kW/m^2 heat flux is expected on wing leading edge. CFD results also indicate that the flow remains laminar on the leeside of fuselage and wing, while on vehicle windside roughly a factor two on heat flux due to turbulence effects is expected. In conclusion, the EFTV's forebody region has resulted critical from the thermal point of view due to the high slenderness of the glider aeroshape, with sharp leading edges for both fuselage nose and wing.
The aerodynamic activities ended with a CFD study of the effects of micro-aerothermodynamics on EFTV aerodynamic performance, by modelling geometrical details (hingeline gap, torsion-bar cavity, wing-aileron fixation and antennas) not included in CFD simulations performed to build the EFTV aerodatabase. Results described in Ref. [14] indicate that the effects of micro-aerothermodynamics on global aerodynamics are well within the uncertainty bands of the EFTV aerodatabase.

3.2. Thermal design

Many thermal analyses, relying on both engineering-level and CFD-FEM based analyses [15, 16], have been performed by CIRA in order to assess different classes of materials. Only the thermal study for the hot aeroshell structure is addressed here, whereas the thermal environment for the internal bays and equipment along with their thermal protection sizing are detailed in [17].

The vehicle thermal behavior has been preliminary assessed by means of the Finite Element Method (FEM) implemented in the commercial software ANSYS. A transient analysis along the computed entry path is performed to evaluate the time dependent temperature of the structure. In synthesis the procedure schematically reported in Fig 7 has been carried out:

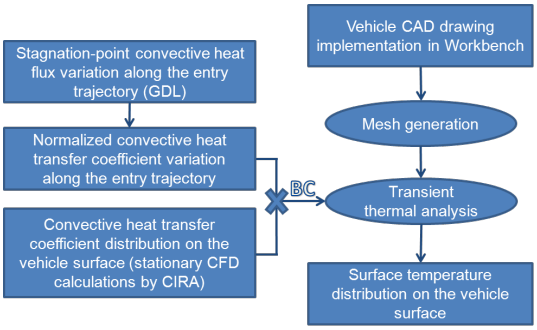

Fig 7. Numerical procedure flow chart

Different classes of materials have been preliminarily selected and analysed for the EFTV structure, namely: titanium alloy, copper, C/C-SiC and zirconia (ZrO_2) for surface coatings.

Titanium alloys exhibit a unique combination of mechanical and physical properties and corrosion resistance which have made them desirable for critical, demanding aerospace applications, also in high temperature conditions. A high temperature resistant copper is employed as a heat sink to accommodate the thermal energy on the nose. C/C-SiC developed at DLR and tested in different high temperatures applications (e.g. HIFiRE and SHEFEX) is considered for ailerons and for the largest part

of the wing leading edge. A zirconia coating layer has been also foreseen to protect some titanium and copper components, increasing the surface emissivity and partly confining the larger temperatures on the layer itself.

In the end, the following assumptions have been carried out on the vehicle components (see Fig 8):

- Nose: copper coated by 1 mm of ZrO_2 on the leading edge and windward, tailoring to 0 mm before mechanical connections with the main structure of the fuselage;
- Wing front part (junction with the nose): titanium coated by 2 mm of ZrO_2 tailoring to 0 mm moving towards the main structure of the fuselage on the leeward;
- Ailerons and wing leading edges: C/C-SiC;
- Remaining parts of titanium alloy structure.

In addition, high emissivity paint (emissivity coefficient ε=0.88) has been applied on the EFTV metallic wet surfaces, even on zirconia coating [18].

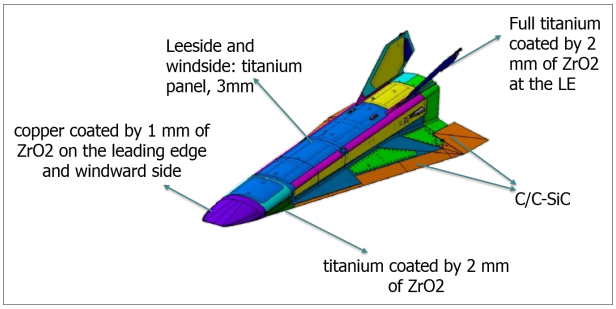

Fig 8. Final TPS configuration

More details on the TPS design procedure and the implementation in the FE model are given in [8].
Fig 9 shows temperature maps when the maximum temperature occurs, i.e. at 290s. No thermal criticalities are highlighted for the different materials.
Fig 10 shows temperature maps at 390s. At this instant the global maximum is lower but the structure is much hotter. This time instant was chosen as load case DPL-2 for thermo-structural analysis (see section 3.4, Table 4).

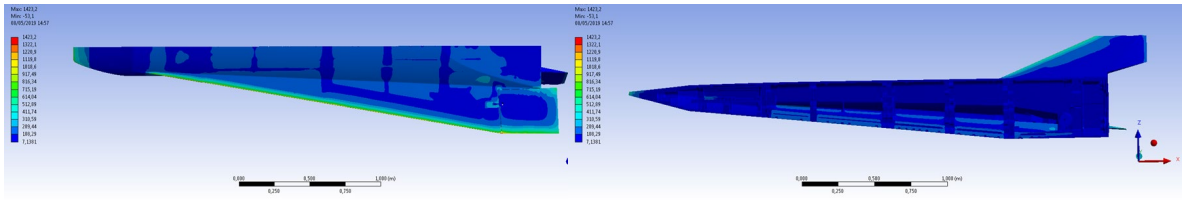

Fig 9. EFTV windward (left) and internal (right) temperature maps at 292s (maximum occurring instant)

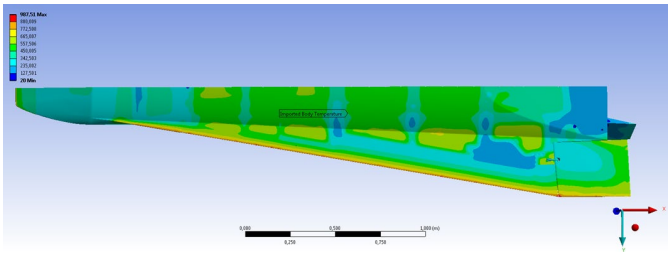

Fig 10. EFTV windward temperature map in re-entry phase at 390s

Contour plots clearly show that zirconia coatings, C/C-SiC and copper components on EFTV (having maximum service temperatures, respectively, in the order of 2400°C, 1600°C and 800°C) would generally widely survive the aerothermal environment in these conditions.
Nevertheless, some components must be studied with particular attention because high thermal gradients are reached on the main structure; among these, in particular the nose tip must be checked.

Nose tip contour plot at maximum trajectory instant (t=409s) is plotted in Fig 11.
Results show that the present configuration is safe from the thermal point of view, but an accurate thermo-structural assessment is necessary due to the combined effect of elevated thermal gradient and poor mechanical properties of copper at elevated temperatures. The joint area between the copper nose and the titanium upper and lower panel must be carefully investigated.

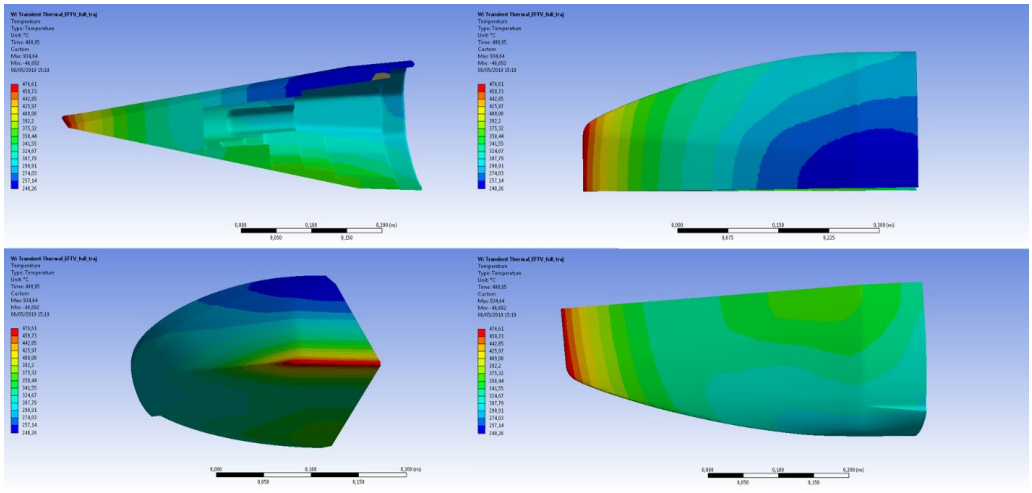

Fig 11. Nose temperature map (maximum occurring at t=409s)

3.3. Structural loads and stress analysis

The EFTV cold structure is composed mainly by the following major items: fuselage, wings and fins (see Fig 12).
The fuselage structure is mainly composed by milling frames, upper beams and panels. The assembly of fuselage structure is realized by joining upper beams, frames and lower panels with fixed bolts, the upper panels are joined to the frames and upper beams by removable bolts in order to allow the access inside of the fuselage for the installation of internal equipment.
The rear fuselage is composed by two shells and a rear panel. The upper part is joint with a bolted strap, the bottom with an overlap between the two shells also bolted with fixed bolts. The rear panel is bolted with removable bolts to allow the access to the internal part of fuselage; holes are also foreseen for the installation of separation devices (for EFTV-ESM separation, see Fig 13).

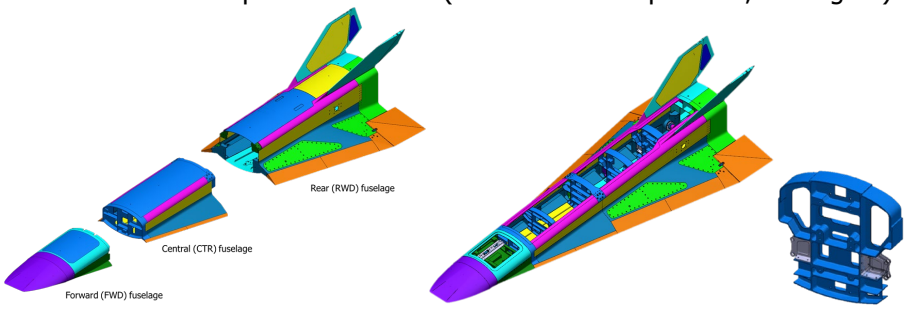

Fig 12. From the left: fuselage main components; global structural view, frame detail

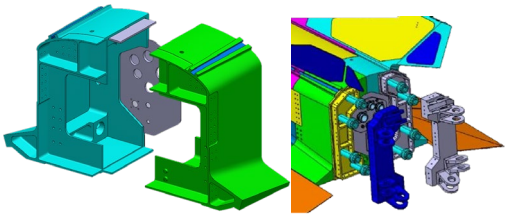

Fig 13. Detail of the base of the EFTV and of the fitting for ESM connection and separation devices installation

3.4. Finite Elements Model and Structural Loads

The loads evaluation and structural analysis have been performed on the basis of the detailed finite element model of the complete vehicle, as shown in Fig 14.

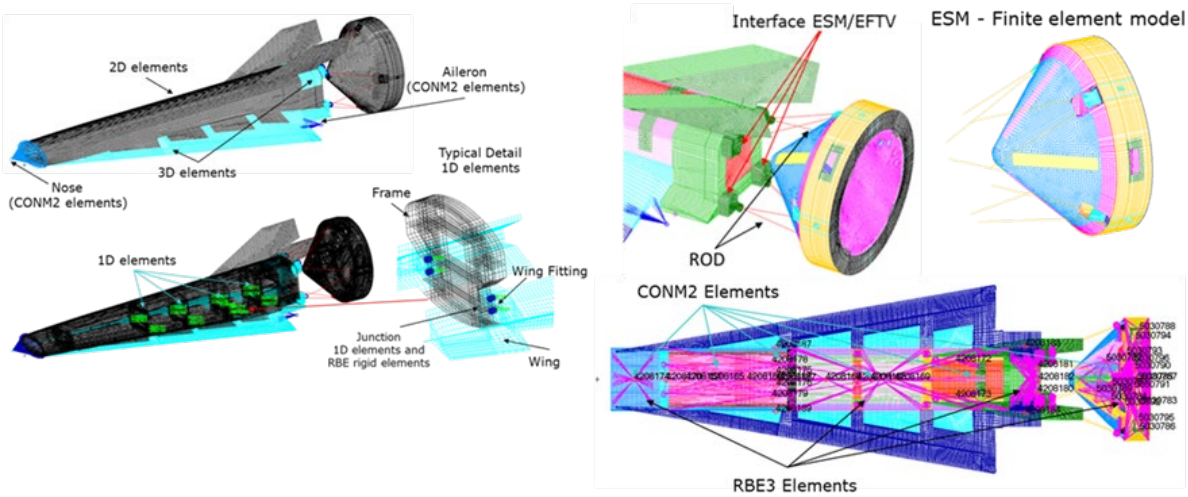

Fig 14. FE Model by Tecnosistem Engineering and Technology (TET)

Structural loads have been defined by means of a dedicated loop analysis, carried out in order to match all requirements.
Two different approaches have been defined for ascent and descent phases to consider that the vehicle is subjected mainly to launcher environment during ascent, such as a payload or a satellite, and to typical manoeuvre' s loads during the descent phase, such as an airplane.
For what concerns the launcher loads, the first step in performing a dynamic analysis is determining the natural frequencies and mode shapes of the constrained structure with damping neglected. These results characterize the basic dynamic behaviour of the structure and are an indication of how the structure will respond to dynamic loading.
In order to obtain a correct dynamic behaviour of the structure, a number of modes so that the total effective modal mass of the model is at least 95% of the actual mass, has been evaluated. The modes with the significant modal effective mass fraction are reported in Table 2.

In order to evaluate the dynamic loads due to launcher environment, a number of frequency response analyses, three for sinusoidal input (one for each direction, see Fig 15-left) and three for random input (one for each direction, see Fig 15-right), were performed by using a modal approach.
The static and dynamic behaviour of the vehicle has been assessed by means of the 3D Finite Element Dynamic Model implemented in the software MSC Nastran.
A frequency response analysis has been performed by using a modal approach, i.e. by taking into account a number of modes so that the total effective modal mass of the model is at least 95% of the actual mass. The modal parameters (i.e. natural frequencies and eigenvalues) of the vehicle have been evaluated with respect to launcher requirements, in order to avoid any coupling effects. The vehicle has been stiffened in order to reach the first natural frequency of 10 Hz.

During the launch the structure is subjected both to the dynamic and static loads. The effect of these different loads can overlap and this requires a suitable combination. Because of the different nature of the two mentioned loads (static and dynamic), an equivalent quasi-static load (typically expressed as equivalent accelerations at the CoG) is computed (Flight Limit Loads). Then, the Design Limit Loads have been obtained by applying the design factor $K_M*K_P*K_Q$ [19] set to 1.5 for the current phase of the project (see Table 3 and Fig 16), where:

- K_M model factor: accounts for uncertainties in mathematical models used to predict dynamic response and loads;
- K_P project factor: accounts for uncertainties due to the maturity status of the program;
- K_Q qualification test factor: used to define the qualification test loads.

Table 2. Natural Frequencies and Modal Effective Mass Fractions; excitation along x, y, z axes

		Modal Effective Mass Fraction [%]		
MODE ID	**FREQUENCY [Hz]**	**X**	**Y**	**Z**
1	8.25	0.000%	**39.035%**	3.169%
2	8.36	0.010%	3.291%	**38.676%**
3	15.21	0.0210%	0.004%	**11.472%**
4	15.32	0.000%	**11.503%**	0.002%
27	43.92	0.468%	0.049%	**14.526%**
28	45.45	0.102%	**19.6763%**	0.012%
32	47.60	**8.037%**	0.056%	0.001%
68	76.49	**71.323%**	0.008%	0.100%
…	…	…	…	…
908	425.19	0.0060%	0.002%	0.000%
TOTAL		**95.00%**	**97.88%**	**97.74%**

Fig 15. Frequency Response Analysis Results for main three directions due to Sinusoidal Input (left) and to Random Input (right)

During the descent phase, the vehicle structure is submitted to: pressure loads due to flight manoeuvres, stresses due to temperature gradients and inertial loads.

To select the most critical trajectory points, two trajectories were compared in terms of load factors (Fig 17): a reference planar trajectory (B-viscous) and a three-dimensional curved trajectory (CIRA 3 DOF and 6 DOF). Two sizing points have been selected from CIRA trajectories 3dof and 6dof: the point corresponding to the pull-out manoeuvre, where Nz=7.3 g and the bank where Ny=2.17g. On the same figure, the CFD points available are reported (black squares); the CFD solutions provide the pressure loads to be composed with the inertial ones.

In particular, the solution at about 300 s, has been combined with the inertial pull-out load and the solution at 350 s with the bank.

Table 3. Design factors for descent and ascent loads

					Descent Phase	**Ascent Phase**
		K_M	**K_P**	**K_Q**	**K_M*K_P**	**K_M*K_P*K_Q**
Project Phase	**PDR**	1.2	1.2	1.25	1.44	1.80
	CDR	1.1	1.1	1.25	1.32	1.50
	QR	1.0	1.0	1.25	1.00	1.25

Flight Limit Loads [g]		
X Direction	Y Direction	Z Direction
± 46.95	± 16.89	± 18.57
± 46.95	± 16.89	± 16.57
± 46.95	± 14.89	± 18.57
± 46.95	± 14.89	± 16.57
± 26.95	± 16.89	± 16.57
± 26.95	± 16.89	± 18.57
± 26.95	± 14.89	± 18.57
± 26.95	± 14.89	± 16.57

Design factor

Design Limit Loads [g]		
X Direction	Y Direction	Z Direction
± 70.43	± 25.34	± 27.86
± 70.43	± 25.34	± 24.86
± 70.43	± 22.34	± 27.86
± 70.43	± 22.34	± 24.86
± 40.43	± 25.34	± 24.86
± 40.43	± 25.34	± 27.86
± 40.43	± 22.34	± 27.86
± 40.43	± 22.34	± 24.86

Fig 16. Load Conditions during ascent due to Dynamic and Static Combination

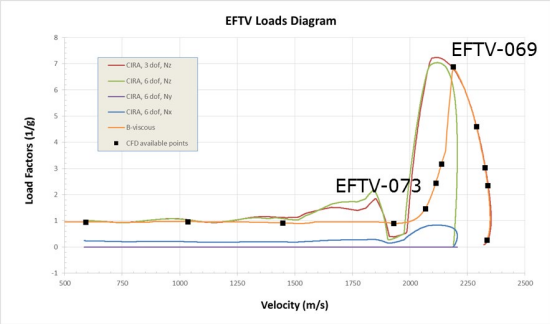

Fig 17. Load Factors for different trajectories

For what concerns temperatures, two sizing cases have been selected:

- Point of maximum stagnation point heat flux (Q_{st}), corresponding to t=300 s;
- Point of maximum temperature on the frames, corresponding to t=390 s from the separation.

A specific procedure has been set-up to interpolate pressures and temperatures results on the structural FE model; the final combination defining the two sizing cases for the descent phase is summarized in Table 4.

Table 4. Descent Phase Loads (DPL) combination

Sizing case	Pressure field (CFD)	Temperature field (thermal analysis)	Inertial Load
DPL-1	EFTV-069 (t=300.5s)	Max Qst (t=300s)	Nz=7.3g
DPL-2	EFTV-073 (t=350s)	Max Tframes (t=390s)	Ny=2.17g

It must be underlined that these loads follow the design approach described above:

- Pressure loads resulting from the interpolation procedure must be multiplied by the design factor identified in Table 3;
- Temperatures have already margins included.

3.5. Stress analysis

Starting from the load conditions described in the previous paragraph, the stress analysis has been performed by TET based on the detailed finite element model of the complete vehicle (EFTV+ESM). Static linear analysis has been performed by the MSC Nastran in order to calculate the distribution of displacements, internal forces and stresses. The internal forces extracted from the FE model have been used for the detailed structural analysis of the main structural components as interface fittings, wing fittings, etc.
Safety Margins have been defined according to ECSS standard:

Table 5. Factors of safety according to [19]

	Verification by analysis only			**Verification by test**		
Structure	FOS_y, Yield	FOS_U, Ult.	FOS_I, Instability	FOS_y, Yield	FOS_U, Ult.	FOS_I, Instability
Metallic	1.25	2.0	2.0	1.1	1.25	1.25
Joint	N/A	2.0	N/A	N/A	1.25	N/A

For each load case, the distribution of displacements, forces and stresses in FE model has been calculated. The maximum stress has been then compared with the allowable one in order to obtain the safety margins.

Some results related to the loads condition during the ascent phase (Fig 16) are reported in Fig 19. All safety margins result positive. In some areas, some critical issues have been investigated in order to guarantee the global safety of the vehicle.

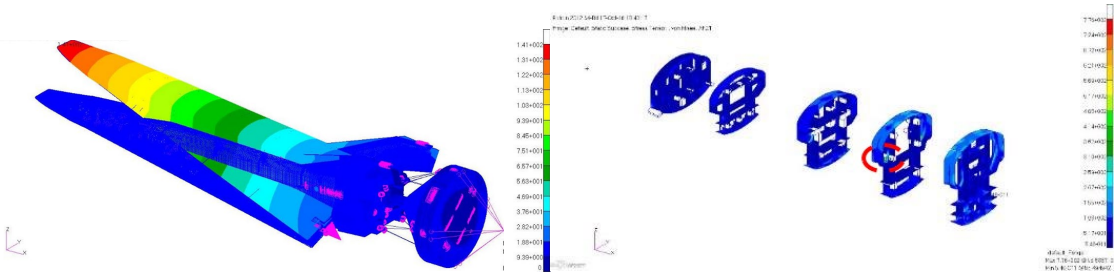

Fig 18. Results of stress analysis. Left: maximum displacement (mm) – Right: maximum stress on frames (MPa)

The second load conditions analysed are the ones reported in Table 4 for the Descent. These load cases take into account also the temperature contribution on total stress. Just as an example, some results related to the condition DPL- 2 of Table 4 (the most demanding one for the descent phase) are shown in Fig 20 and Fig 21. Several items have resulted critical; positive safety margins have been then obtained locally increasing the thickness.

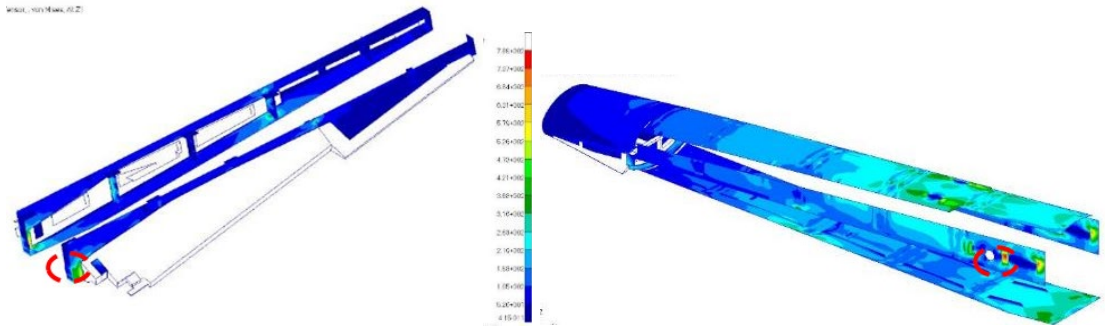

Fig 19. Results of stress analysis. Left: maximum stress on wings (MPa) – Right: maximum stress on panels (MPa)

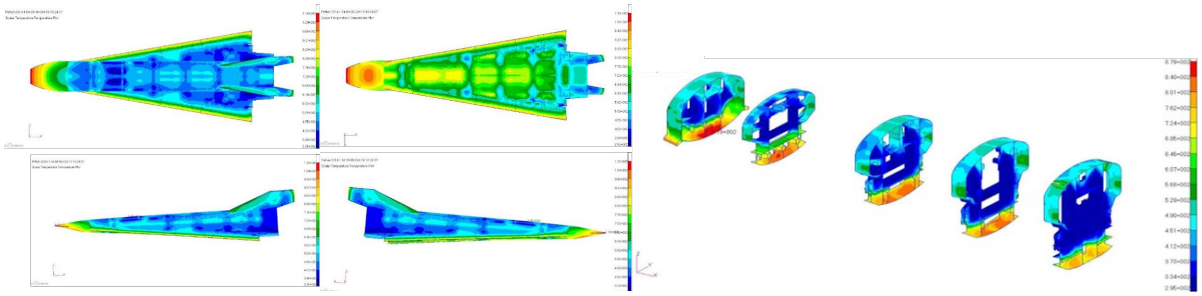

Fig 20. Results of stress analysis under DPL-2 conditions; temperature distribution (K) on vehicle surface (left) and frames (right)

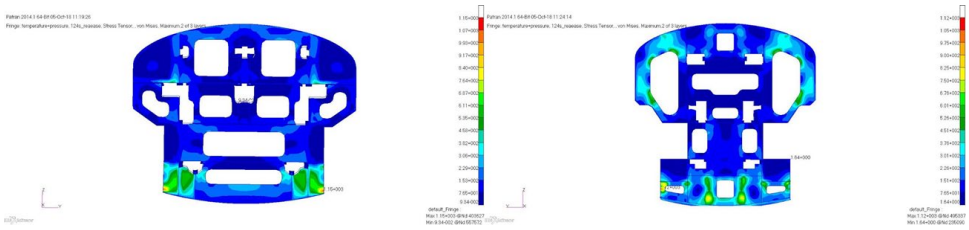

Fig 21. Results of stress analysis under DPL-2 conditions; maximum stress (MPa) on frames

3.6. EFTV Guidance

The EFTV shall perform a flight above Mach 7, maximizing the aerodynamic efficiency in a specified altitude range and in a quasi-levelled flight. Additional constraints are defined for the lateral manoeuvre, due to safety and/or telemetry reasons. This information drove the definition of objectives and constraints of the trajectory.

3.7. EFTV trajectory

The trajectory has been obtained with the aim of achieving different goals depending on the EFTV flight phase while satisfying all the trajectory constraints. The optimization of the AoA profile has been carried out considering a fixed bank angle profile, computed as it will be explained shortly in the following. The nominal angle of attack profile is reported in Fig 22-left.
For what concerns the lateral trajectory, a bank angle reference profile has been computed. The bank angle must consider the constraints concerning the horizontal trajectory. More specifically, they are:

- Distance from Alcantara, Fortaleza or Natal lower than 600 km (for telemetry constraints).
- Final heading angle= -80 deg (EFTV towards Natal at the end of flight).
- Error on final heading angle < 2 deg.

Therefore, the value of the reference bank angle will be computed according to the following logic:

$$\sigma_{cmd} = \begin{cases} \sigma_{\max} * sign(\psi - \psi_{des}) & if \ |\psi - \psi_{des}| > \psi_{th} \\ k_{\Psi}(\psi - \psi_{des}) & if \ |\psi - \psi_{des}| < \psi_{th} \end{cases} \quad [1]$$

where ψ_{des} is the desired final heading, ψ_{th} is a positive threshold, k_{Ψ} is a gain and $sign$ represents the signum function, while $\sigma_{\max}$ is the constant bank angle at which the manoeuvre begins.
The following nominal bank angle command is obtained (Fig 22-right).

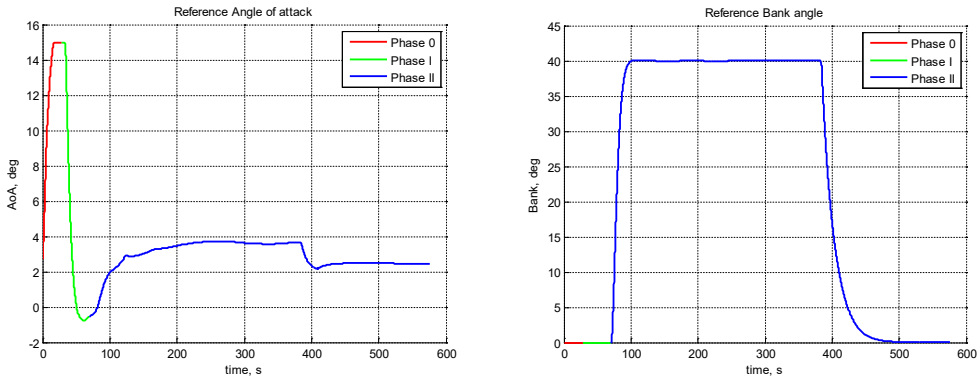

Fig 22. Reference Angle of attack (left) and Reference Bank Angle (right)

3.8. Guidance Laws

Longitudinal guidance laws have the aim of tracking the EFTV reference altitude. In particular, they provide an AoA command to the Flight Control Laws described subsequently. More in detail, it is possible to obtain the following expression for the vertical acceleration:

$$\ddot{h} = \frac{L}{m}\cos\sigma\cos\gamma - \frac{D}{m}\sin\gamma - g \quad [2]$$

where g is the gravity acceleration, m is the vehicle mass, γ is the flight path angle w.r.t the local horizontal plane and positive up, h is the altitude on Earth surface, σ is the bank angle, positive when oriented to the right of the velocity vector, L and D are the lift and drag forces, respectively.
Therefore, it is possible to ensure that a given altitude profile is followed by computing the commanded AoA through feedback linearization. In fact, the AoA (upon which the lift and drag forces depend) can be computed such that

$$\ddot{h} = \ddot{h}_{ref} + k_{h_1}\left(\dot{h}_{ref} - \dot{h}\right) + k_{h_2}\left(h_{ref} - h\right) \quad [3]$$

In this way, the error dynamics will be:

$$\ddot{e}_h + k_{h_1}\dot{e}_h + k_{h_2}e_h = 0 \quad [4]$$

where $e_h = h_{ref} - h$.

3.9. Simulation Results

The used 3Dof flight simulator accepts, as MCI information, the mass and the CoG position. Simulations end at Mach 2, being the limit of the AEDB validity.

A Monte Carlo simulation campaign (1000 runs) has been carried out by using the abovementioned 3DoF simulation model, accepting AoA and bank angle as external inputs. The considered sources of uncertainty are listed below:

- Uncertainties on EFTV initial state due to the propagation of errors and uncertainties from the previous mission phases (launch phase and EFTV-ESM flight from 90 km to 55 km).
- MCI uncertainties (Mass and CoG position).

- AEDB uncertainties.
- Environment Uncertainties (only atmospheric density).
- Errors on tracking of AoA and bank angle. There errors are due to the fact that 3 DoF model does not include control laws as AoA and bank angle are input for the model; however, the presence of a control system has been simulated by applying an error between the commanded AoA (bank angle) and the actual one, that is the one going directly into the 3Dof equations.

Time-histories of flight parameters are reported in the figures below: in blue the nominal values, while the off-nominal ones are superimposed in black, and some of the constraints are indicated in red.

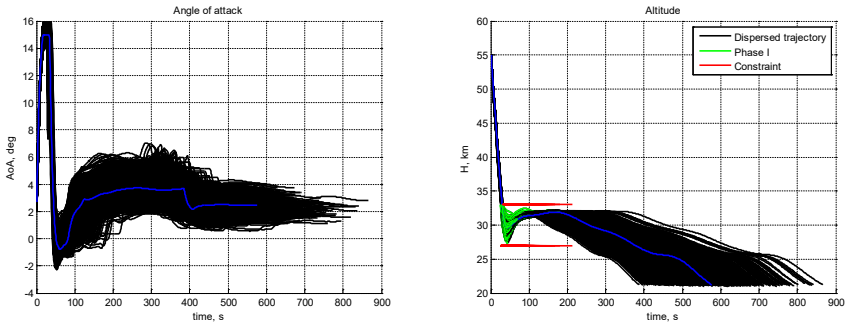

Fig 23. Angle of attack (left) and altitude (right) as a function of time

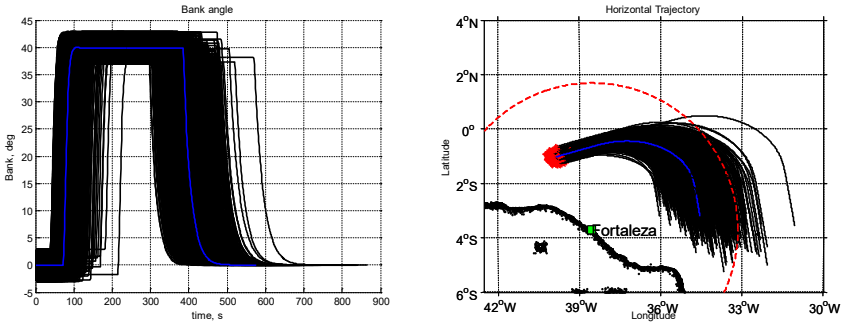

Fig 24. Bank angle as a function of time (left) and Horizontal Trajectory (right)

In spite of large uncertainties, almost all the trajectory constraints are satisfied in dispersed conditions. Actually, the only requirements that cannot be satisfied are the following ones:

- Trimmability: in about 8% of simulations the trimmability is not guaranteed for elevon deflection in the range [-20,10] deg. This happens for high AoA where, in presence of uncertainties, elevon deflection may not be sufficient to trim the EFTV.
- Aerodynamic efficiency during phase I: nominal trajectory has a max L/D which is greater than the minimum required (4); however, as a consequence of AEDB uncertainties, constraints is not satisfied in 48% of runs.
- Distance from telemetry stations: there is a given number of trajectories which lie outside the region in which telemetry coverage is guaranteed (2%).

3.10. EFTV Control Laws

The flight dynamics model used for Control Laws design has been built starting from the equations describing the rotational dynamics. The designed control law is based on a full-state feedback, i.e.:

$$u_{cmd} = \bar{u} - Kx \qquad [4]$$

where x is the state vector and u is the control vector. Control matrix K is computed through LQR technique [23]. Actually, in order to cope with disturbances and modelling errors, an integrator is added on the output (LQI) thus improving the overall tracking performances. Longitudinal and latero-

directional dynamics have been considered separately and two different control laws have been designed. Longitudinal state variables are $\delta x_{long} = [\alpha - \bar{\alpha}, q, -\int \alpha - \bar{\alpha}]$, where $\bar{\alpha}, \bar{\varphi}$ are the trim values of the angle of attack and the roll angle respectively. The control input is $\delta u_{long} = \delta_{elev} - \delta_{trim}$, where δ_{trim} is the trim elevator deflection.

Lateral-directional state variables are $x_{lat} = [\beta, \varphi - \bar{\varphi}, p, r, -\int \varphi - \bar{\varphi}]$, where $\bar{\varphi}$ is the trim value of the roll angle. The control input is $\delta u_{lat} = \delta_{ailer}$.

For each different flight condition, the system to be controlled must be linearized and the LQI problem must be solved (i.e. control gains are computed). Each flight condition is specified by the variables upon which the matrices of linearized system depend.

3.11. Simulation results

The inputs are the same used for the analysis described in sec. 3.9. A Monte Carlo simulation campaign (250 runs) has been carried out by using a complete 6 Dof simulation model. The applied sources of uncertainty are listed below:

- Uncertainties on EFTV initial state, i.e. the difference between nominal EFTV state and actual one, due to the propagation of errors and uncertainties from the previous mission phases (launch phase and EFTV-ESM flight from 90 km to 55 km).
- MCI uncertainties (Mass, CoG position and Inertia matrix).
- AEDB uncertainties.
- Environment Uncertainties (atmospheric density and winds).
- Measurement Errors.
- Actuation System errors.

In the following figures the results of 6 DoF Monte Carlo simulations are reported, where again the blue line represents the nominal trajectory.

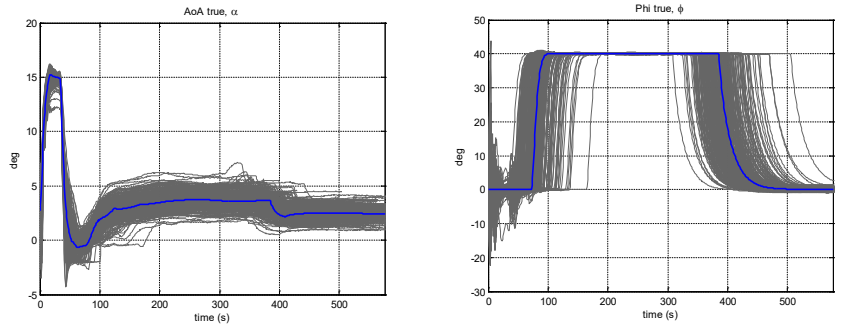

Fig 25. Angle of attack (left) and roll angle (right). Blue lines are the nominal ones.

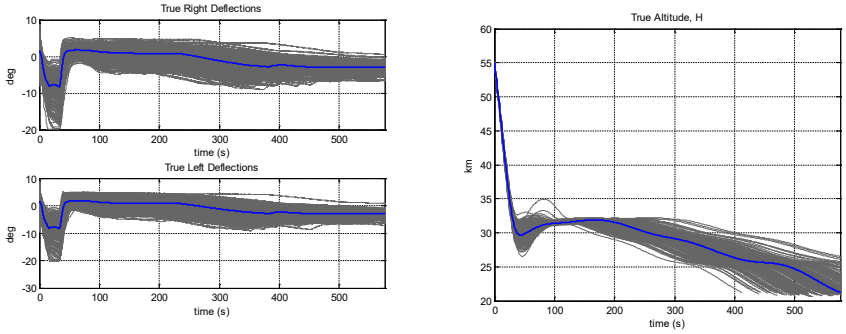

Fig 26. True Deflections (left) and true altitude (right). Blue lines are the nominal ones.

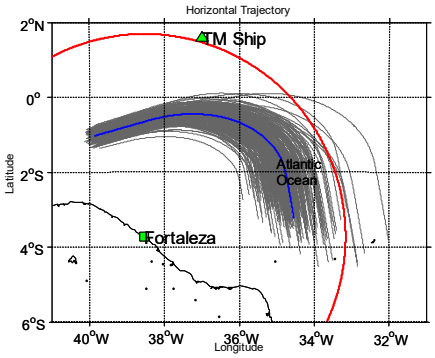

Fig 27. Horizontal Trajectory (blue is the nominal one)

From Monte Carlo results, whose aim was to verify the performances of the guidance and control laws, the following remarks can be done:

- Both Longitudinal and Latero-directional control laws guarantee good tracking of angle of attack and roll angle, except for the first 60 seconds of flight where several manoeuvres are accomplished.
- Altitude tracking accomplished through the longitudinal guidance laws guarantees good performances along the trajectory.
- Lateral guidance is effective in guaranteeing that EFTV is kept towards Natal at the end of flight.

Some trajectory constraints are not satisfied, in particular:

- Aerodynamic efficiency during phase I**:** nominal trajectory has a max L/D which is greater than the minimum required (4); however, as a consequence of AEDB uncertainties, constraints is not satisfied in 56.4% of runs.
- Distance from telemetry stations: there is a given number of trajectories which lie outside the region in which telemetry coverage is guaranteed (0.8% of runs).

4. Conclusions

The design of space mission and vehicle is characterized by continuous interactions between engineering disciplines and therefore a multidisciplinary approach is strongly needed.
The approach presented in this work involves several disciplines, i.e. aerodynamics, aerothermodynamics, loads analysis, materials and structures, flight mechanics and GNC, that work together coordinated by the system authority to fulfill mission and system requirements, and is based on the tight interaction between subsystems up to whole design completion.
The approach has been applied to the HEXAFLY-INT project, with the final aim to demonstrate the technical feasibility of concepts and technologies for the hypersonic flight and then to increase the Technology Readiness Level (TRL) of the breakthrough technologies on board.

Acknowledgments
This work was performed within the 'High Speed Experimental Fly Vehicles - International' (HEXAFLY-INT) project fostering International Cooperation on Civil High-Speed Air Transport Research. HEXAFLY-INT, coordinated by ESA-ESTEC and supported by the European Commission EU within the 7th Framework Program Theme 7 Transport, Contract no.: ACP3-GA-2014-620327.
The project is also supported by the Ministry of Industry and Trade, Russian Federation. Further information on HEXAFLY-INT can be found on http://www.esa.int/techresources/hexafly_int.

References

1. Steelant J., 'Evolutionary Technology Developments towards an International Flight Platform for High-Speed Transportation', Aviation in Europe Innovating for Growth, Proceedings of the 7th European Aeronautics Days, ed. D. Knoerzer et al., 20-22/10/2015, London, UK, doi:10.2777/62810.
2. Steelant J., Villace V., Kallenbach A., Wagner A., Andro J.-Y., di Benedetto S., Saracoglu B. Chernyshev S.L., Gubanov A. A., Talyzin V. A., Voevodenko N. V., Kukshinov N.V., Prokhorov A. N., Grigoriev N. V., Neely A. J., Verstraete D. and Buttwsorth D., 'Flight Testing Designs in HEXAFLY-INT for High-Speed Transportation', 1st International Conference on High-Speed Vehicle Science and Technology (HiSST), HiSST-2018-3101064, 26-29 November 2018, Moscow, Russia.
3. Steelant J., 'Achievements obtained for sustained hypersonic flight within the LAPCAT project', 15th AIAA International Space Planes and Hypersonic Systems and Technologies Conference. Dayton, OH, AIAA 2008-2578, 2008.
4. Steelant J., Varvill R., Defoort S., Hannemann K. and Marini M., 'Achievements Obtained for Sustained Hypersonic Flight within the LAPCAT-II Project', 20th AIAA International Space Planes and Hypersonic Systems and Technologies Conference, AIAA-2015-3677, Glasgow, UK, 6-9 July 2015.
5. Steelant J., 'Achievements obtained on Aero-Thermal Loaded Materials for High-Speed Atmospheric Vehicles within ATLLAS', AIAA-2009-7225, 16th AIAA/DLR/DGLR International Space Planes and Hypersonic Systems and Technologies Conference, Bremen, Germany, October 19-22, 2009.
6. Bouchez M., Crampon F., Le Naour B., Wilhelmi C., Bubenheim K., Kuhn M., Mainzer B., Jiccius J., Davoine C., Justin J.-F., von Wolfersdorf J., Abdelmoula M., Villace-Fernandez V. and Steelant J., 'Combustor and Material Integration for High Speed Aircraft in the European Research Program ATLLAS-II', 19th AIAA Hypersonic Space Plane Conference, Atlanta, Georgia, USA, AIAA-2014-2950.
7. Steelant J., Langener T., Di Matteo F., Hannemann K., Riehmer J., Kuhn M., Ditter C., Scheuerpflug F., Jung W., Marini M., Pezzella G., Cicala M., Serre L., 'Conceptual Design of the High-Speed propelled Experimental Flight test Vehicle HEXAFLY', AIAA 2015-353, 20th AIAA International Space Planes and Hypersonic Systems and Technologies Conference, 6-9 July 2005, Glasgow, UK.
8. Di Benedetto S. et al., 'The high-speed experimental flight test vehicle of HEXAFLY-INT: a multidisciplinary design', CEAS Space Journal, https://doi.org/10.1007/s12567-020-00341-5.
9. Pezzella G., Marini M., Reimann B. and Steelant J., 'Aerodynamic Design Analysis of the HEXAFLY-INT Hypersonic Glider', 20th International Space Planes and Hypersonic Systems and Technology Conference, AIAA-2015-3644, 6-9 July 2015, Glasgow, UK**.**
10. Marini M., Pezzella G., Schettino A., Di Benedetto S., Fernandez-Villace V., Steelant J., Gubanov A.A., Voevodenko N.V., Reimann B. and Walton C., 'Numerical and Experimental Characterization of the HEXAFLY-INT Hypersonic Glider', 21st International Space Planes and Hypersonic Systems and Technology Conference, AIAA-2017-2316, 6-9 March 2017, Xiamen, China.
11. Steelant J., Marini M., Pezzella G., Reimann B., Chernyshev S.L., Gubanov A.A., Talyzin V.A., Voevodenko N.V., Kukshinov N.V., Prokhorov A.N., Neely A.J, Kennel C., Verstraete D., Buttsworth D., 'Numerical and Experimental Research on Aerodynamics of High-Speed Passenger

Vehicle within the HEXAFLY-INT Project', 30th Congress of the International Council of Aeronautical Sciences (ICAS), 25-30/09/2016, Daejeon, Korea.

12. Schettino A., Pezzella G., Marini M., Di Benedetto S., Villace V. F., Steelant J., Choudhury R., Gubanov A. and Voevodenko N., 'Aerodynamic Database of the HEXAFLY-INT Hypersonic Glider'. CEAS Space Journal, https://doi.org/10.1007/s12567-020-00299-4.
13. Steelant J., Passaro A., Fernandez-Villace V., Gubanov A.A., Shvalyov Y.G., Ivanyuskhin D.S., Voevodenko N.V., Marini M. and Di Benedetto S., 'Boundary Layer Transition Assessment on a Slender High-Speed Vehicle', 21st International Space Planes and Hypersonic Systems and Technology Conference, AIAA-2017-2133, 6-9 March 2017, Xiamen, China.
14. Choudhury R., Villace V. F., Steelant J., Buttsworth D., Marini M. and Di Benedetto S., 'Micro-Aerothermodynamic Analysis of Protuberances and Clearances on a Hypersonic Glider Using a Reduced Domain Approach', 1st International Conference on High-Speed Vehicle Science Technology (HiSST), HiSST-2018-1100813, Moscow, Russia, November 26-29, 2018.
15. Scigliano R., Carandente V., Favaloro N., Cardone S. and Steelant J., 'Thermo-Structural Design of the HEXAFLY-INT Experimental Flight Test Vehicle (EFTV)', IMECE2015-5093, Int. Mechanical Engineering Congress & Exposition, Nov. 13-19 2015, Houston, Texas, US.
16. Scigliano R., Pezzella G., Di Benedetto S., Marini M., Steelant J., 'HEXAFLY-INT Experimental Flight Test Vehicle (EFTV) Aero-Thermal Design', IMECE2017-70392, Tampa, FL, USA, November 3-9, 2017.
17. Andro J.-Y., Scigliano R., Kallenbach A. and Steelant J., 'Thermal Management of the Hexafly-Int Hypersonic Glider', 1st International Conference on High-Speed Vehicle Science and Technology (HiSST), HiSST-2018-1770921, 26-29 November 2018, Moscow, Russia.
18. Ivankin M., Kazhickhin S., Nikulenko A., Shardin A., Talyzin V. and Steelant J., 'Investigation of the Thermal Protective Coating for the Experimental Flight Test Vehicle within the International HEXAFLY-INT Project', 7th European Conference for Aeronautics and Space Sciences (EUCASS), Milan, Italy, 3-6 July 2017, doi: 10.13009/EUCASS2017-433.
19. ECSS-E-ST-32-10C_Rev.1, 6 March 2009.
20. Munk D. J., Vio G. A., Verstraete D. and Steelant J., 'Structural Topology Optimisation of the HEXAFLY-INT Vertical Fin', 1st International Conference on High-Speed Vehicle Science and Technology (HiSST), HiSST-2018-1760854, 26-29 November 2018, Moscow, Russia.
21. Morani G., Nebula F., Di Donato M. P., Di Benedetto S. and Steelant J., 'Trajectory and Flight Mechanics Analysis of the HEXAFLY-INT Experimental Flight Vehicle', 1st International Conference on High-Speed Vehicle Science and Technology (HiSST), HiSST-2018-1860856, 26-29 November 2018, Moscow, Russia.
22. Andro J.-Y., Nebula F., Rotärmel W. and Steelant J., 'Control and Elevon Actuation Systems of the Hexafly-Int Hypersonic Glider', 1st International Conference on High-Speed Vehicle Science and Technology (HiSST), HiSST-2018-1770922, 26-29 November 2018, Moscow, Russia.
23. Brian D. O. Anderson, John Barratt Moore, "Optimal control: linear quadratic methods", Prentice Hall, 1990.